Novel Additive for Addressing Interfacial Instability in PVDF-HFP/Pyr14FSI Systems for Lithium Metal Batteries at Room Temperature

Battery Energy

WILEY

RESEARCH ARTICLE OPEN ACCESS

Novel Additive for Addressing Interfacial Instability in PVDF-HFP/$Pyr_{14}FSI$ Systems for Lithium Metal Batteries at Room Temperature

Leonardo Balducci[1,2] | Hamideh Darjazi[1,2] | Marisa Falco[1,2] | Camilla Noè[1] | Gérôme Godillot[3] | Giuseppe Antonio Elia[1,2] | Claudio Gerbaldi[1,2]

[1]GAME Lab, Department of Applied Science and Technology (DISAT), Politecnico di Torino, Torino, Italy | [2]National Reference Center for Electrochemical Energy Storage (GISEL) - INSTM, Firenze, Italy | [3]Arkema, Groupement de Recherches de Lacq, Lacq, France

Correspondence: Leonardo Balducci (leonardo.balducci@polito.it) | Claudio Gerbaldi (claudio.gerbaldi@polito.it)

Received: 1 March 2026 | **Revised:** 4 May 2026 | **Accepted:** 9 May 2026

Funding: HORIZON EUROPE Framework Programme, Grant/Award Number: 101147094

Keywords: divinyl sulfone | ionic liquid | lithium metal battery | poly(vinylidene fluoride-co-hexafluoropropylene) | polymer electrolyte

ABSTRACT

Self-standing hybrid solid polymer electrolytes (HSPEs) are herein fabricated through a solvent-free process, enabling energy-efficient and industry-compatible production. The HSPEs are based on a poly(vinylidene fluoride-co-hexafluoropropylene) (PVDF-HFP)/$Pyr_{14}FSI$ ionic liquid (IL) system incorporating a small amount of divinyl sulfone (DVS) as a functional additive. This design delivers high ionic conductivity together with excellent mechanical integrity and thermal stability. The IL promotes efficient ion conduction and contributes to thermal stability, while incorporating DVS in little amounts (up to 5%) effectively stabilizes the solid–electrolyte interface (SEI) layer and mitigates degradation processes commonly observed in PVDF-HFP/$Pyr_{14}FSI$-based systems. This study presents the first demonstration of a PVDF-HFP/$Pyr_{14}FSI$-based electrolyte in which the incorporation of a small amount of DVS enables stable and reversible lithium plating/stripping over 1200 h of continuous cycling at room temperature, with a fixed areal capacity of 0.2 mAh cm^{-2}, in laboratory-scale solid-state lithium metal batteries (SSLMB). Furthermore, laboratory-scale SSLMB cells employing high-energy NMC811 cathodes exhibit excellent electrochemical performance, delivering specific capacities of 120 mAh g^{-1} at C/20 and 100 mAh g^{-1} at C/5 under ambient conditions, thereby advancing the development of high-voltage, intrinsically safe, and high-performance next-generation SSLMB technologies.

1 | Introduction

Lithium-ion batteries (LIBs) have revolutionized portable electronics and become an essential component of modern life [1]. However, the growing global energy demand and the ongoing green transition toward a fully electrified and sustainable society call for next-generation storage devices with higher performance and improved safety [2].

Lithium metal batteries (LMBs) are widely considered a promising successor to LIBs due to their significantly higher energy density. In particular, the lithium metal anode is regarded as the ideal anode material, offering an exceptionally high theoretical specific capacity of 3860 mAh g^{-1} and a low redox potential of −3.04 V versus SHE [3]. However, LMBs employing liquid electrolytes suffer from severe plating and stripping instabilities, leading to uncontrolled dendrite growth and posing serious safety risks due to potential short-circuiting and explosion [4].

To address these challenges, solid polymer electrolyte (SPE)-based systems have emerged as promising candidates for next-generation electrochemical energy storage systems [5, 6]. SPEs offer intrinsic safety advantages, such as reduced flammability and the absence of

electrolyte leakage, while enabling lightweight, flexible, and mechanically compliant battery architectures that can withstand vibration and mechanical stress [7]. Based on their composition and ion-transport mechanisms, polymer electrolytes are broadly classified into two categories: (i) truly (dry) SPEs, in which lithium salts are directly dissolved within a polymer matrix, and (ii) hybrid SPEs (HSPEs), including composite polymer electrolytes (CPEs) and gel or quasi-solid-state polymer electrolytes (GPEs), where inorganic fillers and/or plasticizing agents are incorporated to enhance ionic conductivity and interfacial contact [1]. A key limitation of dry SPEs is their inherently low ionic conductivity at room temperature, typically below 10^{-6} S cm^{-1}, which significantly limits their practical applicability. In this context, a variety of polymer hosts, such as poly(ethylene oxide) (PEO) [8–10], polyvinylidene fluoride (PVDF), poly(vinylidene fluoride-co-hexafluoropropylene) (PVDF-HFP), and poly(methyl methacrylate) (PMMA) [11], have been extensively investigated due to their favorable processability and mechanical flexibility [12–14].

Among these, PVDF-HFP has attracted particular attention as a structural backbone owing to its high mechanical strength, excellent thermal and chemical stability, and ease of processability. However, PVDF-HFP does not function as an efficient ion-conducting medium on its own, as it exhibits low intrinsic ionic conductivity and limited lithium salt solvation capability. Consequently, PVDF-HFP is most effectively employed as a mechanically robust framework in HSPEs, where the mobility of Li^+ ions is primarily provided by incorporated ionic conductors, such as ionic liquids (ILs) or lithium salt–containing phases. PVDF-HFP plays a crucial role in ensuring mechanical integrity and electrochemical stability, making it a valuable component in the development of advanced polymer electrolytes for high-energy-density LMBs [15, 16].

ILs are typically composed of organic cations paired with anions exhibiting highly delocalized charge distributions. In electrochemical energy storage systems, commonly employed cations include imidazolium (Im), pyrrolidinium (Pyr), piperidinium (PP), phosphonium, and linear quaternary ammonium species. The accompanying anions may be either inorganic, such as BF_4^- or PF_6^-, or organic, most frequently fluorosulfonyl imide (FSI^-) or bis (trifluoromethanesulfonyl)imide ($TFSI^-$). In comparison with conventional organic carbonate-based electrolytes, ILs exhibit negligible vapor pressure, elevated boiling points, and enhanced thermal stability. These characteristics enable battery operation over a wider temperature range while significantly mitigating flammability and fire-related risks [17].

In recent years, electrolytes based on PVDF-HFP and incorporating ILs have demonstrated high ionic conductivity at room temperature [2, 18, 19]. Despite this advantage, their interfacial stability with lithium metal, particularly under plating/stripping conditions, remains a significant challenge. The limited capability of PVDF-HFP to effectively confine the liquid phase facilitates IL migration and accumulation at the lithium metal edges. This interfacial buildup accelerates polymer electrolyte degradation, reduces ionic conductivity, and can ultimately lead to internal short-circuiting.

A promising strategy to mitigate these issues involves the introduction of suitable electrolyte additives capable of suppressing parasitic side reactions, thereby stabilizing the lithium metal surface through the formation of a thin, uniform, and stable solid electrolyte interphase (SEI) layer. Among the various additives investigated, divinyl sulfone (DVS) has been reported in LIB systems as an effective SEI-forming additive, facilitating interfacial stabilization and improved charge-transfer processes. To our knowledge, however, the application of DVS in LMB systems has not yet been explored [20–22].

In this study, a solvent-free fabrication approach was developed for fabricating PVDF-HFP/IL HSPEs that simultaneously deliver high ionic conductivity at room temperature and enhanced interfacial stability with lithium metal under long-term operating conditions. The incorporation of DVS was specifically designed to facilitate the formation of a stable and protective SEI at the lithium metal anode, thereby suppressing interfacial degradation [4, 23, 24]. The role of DVS was assessed at two different additive concentrations and investigated using electrochemical impedance spectroscopy (EIS) and lithium plating/stripping experiments. In addition, HSPEs were characterized by thermal and vibrational spectroscopic techniques to provide a comprehensive evaluation of the structural phase and concentration of the constituents. The results demonstrate that the controlled introduction of DVS markedly improves the electrochemical performance and interfacial stability of the electrolytes at 25°C. Eventually, the practical applicability was demonstrated by galvanostatic charge/discharge cycling in laboratory scale full LMB cells with a high-energy-density NMC811 cathode, advancing these systems toward practical application in SSLMBs.

2 | Experimental

2.1 | Materials Supply

Poly(vinylidene fluoride-co-hexafluoropropylene) (PVDF-HFP, 85:15, CAS No. 9011-17-0) was provided by Arkema (France). The ionic liquid 1-butyl-1-methylpyrrolidinium bis (fluorosulfonyl)imide ($Pyr_{14}FSI$, CAS No. 1057745-51-3) was provided by Proionic GmbH (Austria). Lithium salt bis (trifluoromethanesulfonyl)imide (LiTFSI, battery grade, CAS No. 90076-65-6) and divinyl sulfone (DVS, CAS No. 77-77-0) were purchased from Solvionic (France) and Merck, respectively. PVDF-HFP was thoroughly dried under vacuum at 60°C for 72 h before use. LiTFSI was subjected to a three-step drying process before use: 24 h under vacuum at room temperature, followed by 48 h at 70°C, and a final 2 h at 110°C. All drying procedures were performed in a Büchi B-585 glass drying oven (Switzerland). All other reagents were used without further purification.

2.2 | Hybrid Solid Polymer Electrolytes (HSPE) Preparation

HSPE were prepared using a truly solvent-free processing method. The pristine HSPE was prepared as follows: $Pyr_{14}FSI$ and LiTFSI were mixed in a stoichiometric ratio of 4:1 in a beaker and stirred at 70°C until complete dissolution of the lithium salt. Separately, the required amount of PVDF-HFP was weighed into a clean Thinky Mixer container. Once the lithium salt was fully dissolved, the $Pyr_{14}FSI$/LiTFSI solution was added to the PVDF-HFP in the mixer at a weight ratio of 20:80 (PVDF-HFP:$Pyr_{14}FSI$ + LiTFSI). The

mixture was homogenized by speed-mixing at 2000 rpm for 2 min, followed by a defoaming step at 1000 rpm for 1 min. The uniform dispersion was then transferred into a beaker and heated to 120°C to induce gelation and form a solid coin. The solid coin was sandwiched between two Mylar layers, one fitted with two Kapton tape spacers, and the assembly was enclosed in a coffee bag for hot pressing. Hot pressing was performed at 120°C for 5 min under 0.5 bar, followed by pressing at 120°C for 5 min under 10 bar, resulting in a transparent, thin HSPE membrane. For the modified HSPEs, DVS was incorporated at 3 wt% and 5 wt%, respectively. To maintain the overall composition, the DVS addition was compensated by a corresponding decrease in the $Pyr_{14}FSI$/LiTFSI fraction while keeping the PVDF-HFP content constant at 20 wt% (Figure 1). In the manuscript, the different formulations will be referred to as pristine, 3% DVS, and 5% DVS, respectively.

2.3 | Structural Characterization

To assess chemical and structural changes, Infrared (IR) spectroscopy was performed on both the precursors and the as-prepared HSPEs. The IR spectra were recorded by Nicolet iS 50 Spectrometer equipped with a single reflection attenuated total reflectance (ATR) tool. Samples were scanned over a range of 4000-500 cm^{-1} with a resolution of 4 cm^{-1}. Data acquisition and processing were carried out using Omnic software (Thermo Fisher Scientific).

Homogeneity and elemental composition were additionally evaluated using energy-dispersive X-ray (EDX) spectroscopy over multiple regions of the HSPE. Analyses were performed with a NeoScope JEOL JCM-7000 scanning electron microscope (JEOL Ltd., Japan) equipped with an EDX detector.

2.4 | Electrochemical Characterization

The compatibility of the HSPEs with lithium metal and their performance during lithium plating and stripping were evaluated using galvanostatic cycling with potential limitation (GCPL) at room temperature in symmetric Li||HSPE||Li cells. The cells were assembled in an inert atmosphere, using 12 mm lithium electrode and 16 mm electrolyte discs in CR2032 coin cells. Cycling was conducted at a current density of 0.1 mA cm^{-2}, with a fixed areal capacity of 0.2 mAh cm^{-2} per half-cycle. This protocol allowed detailed assessment of interface stability, voltage polarization, and plating/stripping behavior over extended cycling.

Ionic conductivity (σ) was measured by electrochemical impedance spectroscopy (EIS) using a VMP-3 multichannel potentiostat/galvanostat (BioLogic, France). Circular HSPE specimens (16 mm in diameter, approximately 100 μm thick) were placed between two stainless steel (SS) blocking electrodes in SS||HSPE||SS cell configurations, which were mounted in standard ECC-Std test holders (EL-CELL, Germany). The thickness of each HSPE was precisely measured before and after testing using a digital micrometer (Mitutoyo). EIS measurements were recorded over a frequency range of 0.1 Hz to 1 MHz with an AC amplitude of 20 mV. The experiments were conducted at temperatures from −20°C to 70°C in 10°C increments using a temperature-controlled environmental chamber (MK 53 E2, BINDER, Germany), allowing the cells to equilibrate for 100 min at each setpoint. Nyquist plots were analyzed with EC-Lab software, and the bulk resistance (R) was determined from the high-frequency intercept. The ionic conductivity (σ) was calculated using the following equations (1)

$$\sigma = \frac{D}{AR} \tag{1}$$

where D is the HSPE thickness (cm), A the electrode area (cm^2), and R the resistance (Ω).

The electrochemical stability window (ESW) of the HSPEs was determined using linear sweep voltammetry (LSV) at room temperature. Measurements were performed in a Li||HSPE||carbon-coated aluminum (CC-Al) configuration, with lithium metal

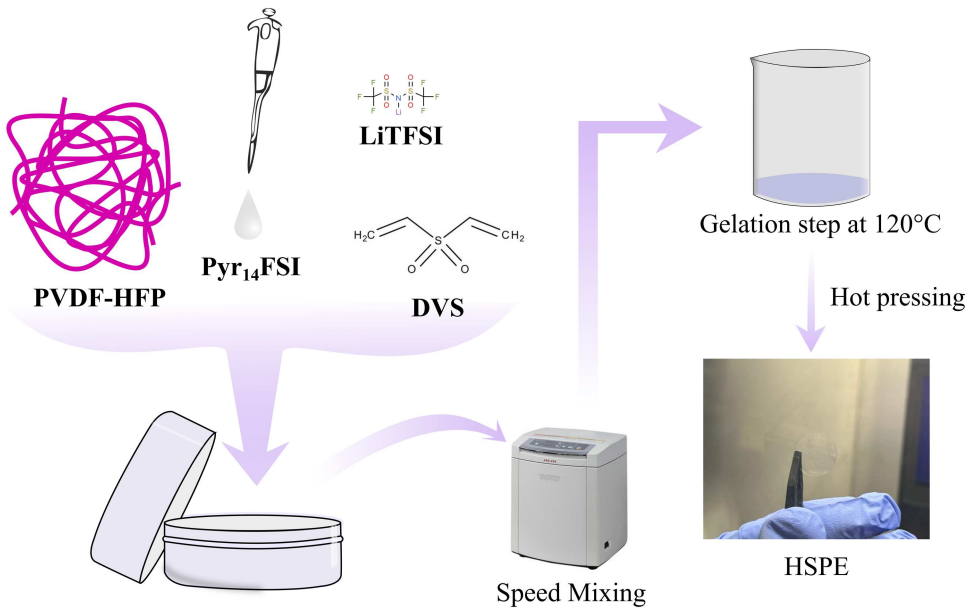

FIGURE 1 | Schematic representation of the preparation process and resulting aspect of HSPEs under study.

(Albemarle) acting as both the counter and reference electrode, and CC-Al serving as the working electrode. The CC-Al electrodes were prepared by casting a slurry containing 80 wt% of conductive carbon black (Super C65, Merck) and 20 wt% of PVdF binder in N-methyl-2-pyrrolidone (NMP, Merck) onto aluminum foil current collector. The coated films were air-dried overnight at room temperature, punched into disks, and subsequently vacuum-dried at 120°C for 24 h to remove residual solvent and moisture. LSV scans were performed from the open-circuit voltage (OCV) up to 6.0 V versus Li^+/Li at a scan rate of 1 mV s^{-1}. The onset of oxidative decomposition was identified as the potential at which the current density exceeded 5 μA cm^{-2}. In addition, chronoamperometry (CA) measurements were conducted at stepwise potentials within the 3.3–4.8 V range to precisely probe the oxidative stability under constant voltage conditions.

To investigate the practical applicability of the HSPEs in full-cell configurations, laboratory-scale SSLMB cells were assembled in a Li‖HSPE‖NMC811 configuration using ECC-Std holders for galvanostatic cycling tests at room temperature. The rate capability was evaluated by cycling the cells at progressively increasing current densities, starting from C/40 and stepping up every five cycles up to C/2 (C/40, C/20, C/10, C/5, and C/2), before returning to C/20. In this study, a 1 C rate was defined as 180 mA g^{-1} relative to the mass of active material in the NMC811 electrode. For the preparation of NMC811 cathodes, PVDF was first dissolved in NMP under constant stirring. Separately, the active material and conductive carbon (Super C65) were thoroughly mixed and ground to form a homogeneous powder blend. This mixture was then added to the PVDF/NMP solution to produce a slurry with a mass ratio of active material:Super C65:PVDF = 90:5:5. Homogenization was achieved using a Thinky Mixer. The resulting slurry was coated onto aluminum foil using a doctor blade with a 200 μm gap. The coated electrodes were initially dried at 70°C for 2 h and then at room temperature. After drying, the electrodes were pressed, cut to the desired dimensions, and vacuum-dried overnight at 120°C. The final cathodes had a thickness of about 30 μm and active material loading of approximately 3 mg cm^{-2}. Electrochemical testing was performed at ambient laboratory temperature (23 ± 2°C) using the VMP-3 potentiostat/galvanostat.

3 | Results and Discussions

3.1 | Structural Analysis of HSPEs

IR spectroscopy in ATR mode was carried out to investigate possible structural modifications induced by the mixing/pressing processes and to assess the purity of the raw precursors (Figure 2). Figure 2a shows the IR spectra of PVDF-HFP, $Pyr_{14}FSI$, and DVS, while Figure 2b compares the IR spectra of all formulated HSPEs (pristine, 3% DVS, and 5% DVS).

As widely reported in the literature, PVDF-HFP exhibits three crystalline phases, namely α, β, and γ. The absorption bands at 1455, 1424, 1265, 1202, together with the sharp peaks at 875 and 842 cm^{-1}, are characteristic of the β phase, whereas the bands at 798 and 698 cm^{-1} are attributed to the α phase [2, 25–27]. Additionally, the most intense peaks at 1411 and 1182 cm^{-1} correspond to C–F and C–C stretching vibrations, respectively, which are common to all crystalline phases [27]. The IR spectrum of $Pyr_{14}FSI$ exhibits the typical absorption bands of the ionic liquid, consistent with literature reports [18, 28, 29]. The IR spectrum of DVS shows weak bands at 3105, 3055, and 3020 cm^{-1} assigned to asymmetric CH_2, CH, and symmetric CH_2 stretching vibrations, respectively. The medium intensity band at 1384 cm^{-1} is attributed to CH_2 bending, while the sharp peaks at 1300 and 1130 cm^{-1} are assigned to asymmetric and symmetric S = O stretching vibrations, respectively. The sharp band at 769 cm^{-1} is ascribed to asymmetric C–S stretching [30, 31]. As shown in Figure 2b, in both pristine and additive-containing HSPEs, the characteristic absorption bands of the α phase vanish, while those of the β phase become more intense. This observation suggests a conformational rearrangement of the polymer chains after the hot-pressing step, favoring the formation of the electroactive β phase [27].

To further investigate the composition of HSPEs and assess the purity of the raw materials, thermogravimetric analysis (TGA) was

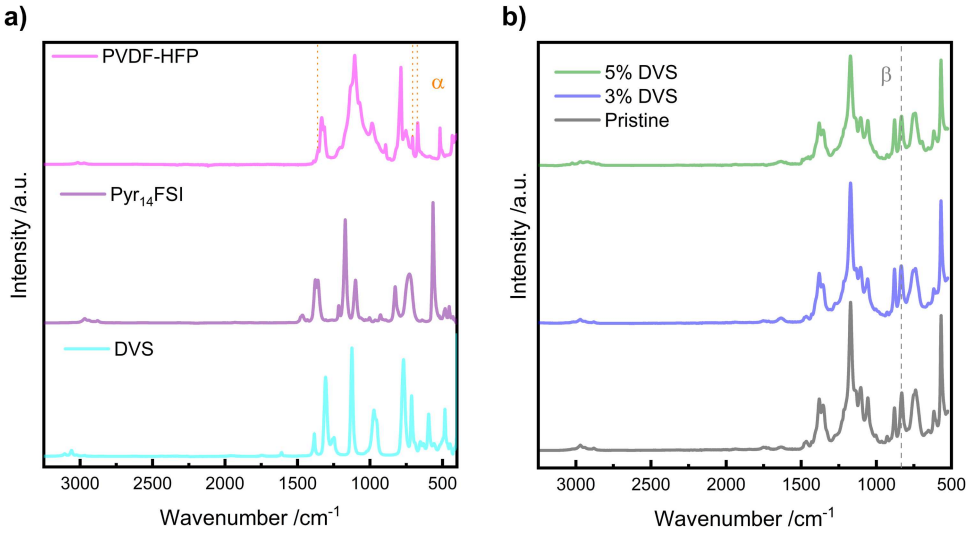

FIGURE 2 | IR spectra recorded in ATR mode of the HSPE precursors PVDF-HFP, $Pyr_{14}FSI$, and DVS (a) and comparative IR spectra of the HSPEs under study, namely pristine, 3% DVS, and 5% DVS (b).

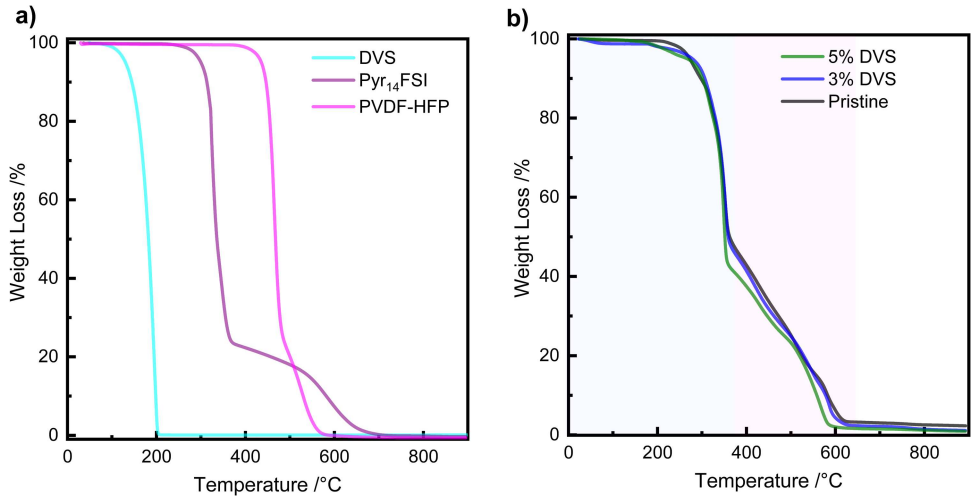

FIGURE 3 | TGA profiles of the HSPE precursors, namely PVDF-HFP, $Pyr_{14}FSI$, and DVS (a), and of the HSPEs under study, including pristine, 3% DVS, and 5% DVS (b).

TABLE 1 | Selective area elemental analysis of the HSPEs under study, namely pristine, 3% DVS, and 5% DVS.

Sample name	C (Mass %)	O (Mass %)	N (Mass %)	F (Mass %)	S (Mass %)	Total
Pristine	38.61	13.38	6.97	26.67	14.37	100
3% DVS	37.32	15.75	6.25	25.98	14.70	100
5% DVS	37.77	17.36	6.13	23.66	15.26	100

performed. Figure 3a shows the TGA profiles of the raw precursors PVDF-HFP, $Pyr_{14}FSI$, and DVS. Both PVDF-HFP and $Pyr_{14}FSI$ show weight loss behavior and degradation temperatures consistent with those reported in the literature [25, 28, 32]. DVS exhibits an initial weight loss attributed to partial polymerization initiated in the presence of oxygen, followed by thermal degradation at temperatures above 120°C and complete volatilization around 200°C [22]. Figure 3b shows the TGA curves of the prepared HSPEs (pristine, 3% DVS, and 5% DVS). Two main degradation regions can be identified: the first region, highlighted in dark blue, is attributed to the degradation of $Pyr_{14}FSI$ and DVS, while the second region, indicated in magenta, corresponds to the degradation of PVDF-HFP and secondary degradation products of $Pyr_{14}FSI$. Although the contribution of DVS to the overall weight loss is difficult to quantify in these systems, little additional weight loss is observed in the temperature range of 130°C-150°C for the HSPEs containing 3% and 5% DVS, respectively, which are in good agreement with the nominal DVS content in the HSPEs.

To further investigate the chemical composition of the HSPEs, EDX elemental analysis was performed. Table 1 lists the mass percentages of the main elements present in the HSPEs. The results show a moderate increase in sulfur and oxygen content in addition to a decrease in the fluorine content, confirming the successful incorporation of DVS into the system.

3.2 | Electrochemical Analysis of HSPEs

To evaluate the interfacial stability of the HSPEs against lithium metal and the effect of DVS incorporation, galvanostatic Li plating/stripping experiments were conducted in symmetric Li||HSPE||Li cells at ambient laboratory temperature. Tests were performed at a current density of 0.1 mA cm^{-2}, with a fixed areal capacity of 0.2 mAh cm^{-2} per plated/stripped half-cycle.

Figure 4a shows the behavior of the pristine HSPE, which exhibits very limited plating/stripping capability, with cell operation lasting no more than 160 h before short-circuiting. Prior to the plating stripping test, the cell was monitored by EIS over time during the OCV. As shown in Figure 4b, cell resistance increases markedly over time, indicating progressive electrolyte degradation, possible leakage, and partial SEI formation. This behavior was further confirmed by disassembling the cell after short-circuiting. As illustrated in Figure 4c, the pristine HSPE exhibits clear signs of degradation, including pronounced color changes induced by lithium plating/stripping. These effects are likely associated with highly acidic and volatile compounds, resulting from interfacial side reactions at the very high current density lithium metal edge and consequential carbonization of the polymer electrolyte.

Figure 5 shows the lithium plating/stripping behavior and Nyquist plots of the HSPEs containing 3% and 5% DVS tested at a current density of 0.1 mA cm^{-2}. Both DVS-containing HSPEs exhibit a significantly extended cycling lifetime, reaching up to 1200 h of stable plating/stripping. Overpotentials of the additive-containing HSPEs are higher than those of the pristine sample, which can be attributed to the formation of a thicker SEI. Moreover, the overpotential increases with increasing DVS content, from 3% to 5%. As shown in Figure 5a, the HSPE containing 3% DVS shows only a modest increase in overpotential, rising from a stabilized value of approximately 0.25 to 0.40 V at the end of the test. In contrast, the HSPE with 5% DVS shows a more pronounced increase, with the overpotential nearly doubling from an initial stabilized value of about 0.35 to

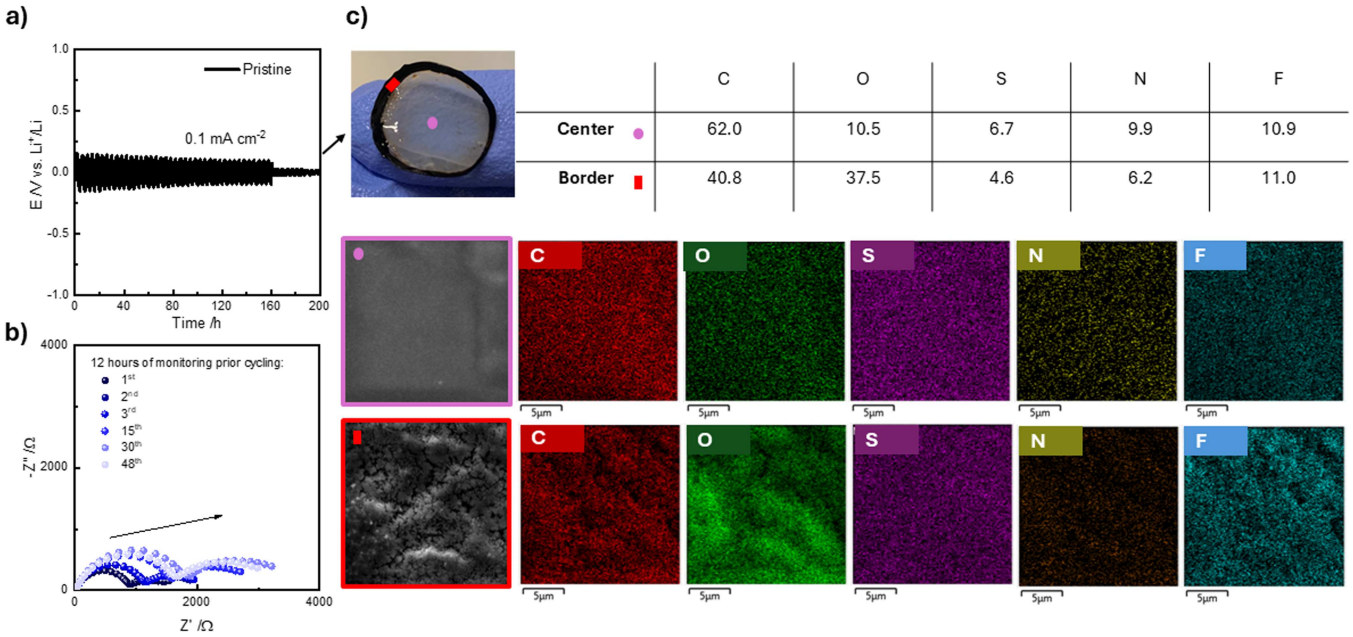

FIGURE 4 | Laboratory temperature long-term galvanostatic lithium plating/stripping cycling of pristine HSPE at a current density of 0.1 mA cm^{-2} (a). EIS spectra obtained at OCV (b). Photograph and EDX elemental mapping of the pristine HSPE after short circuiting (c).

0.60 V. These results suggest that excessive DVS content may adversely affect overall cell performance, likely due to increased interfacial resistance and/or reduced ionic conductivity. Despite these differences, EIS results indicate comparable overall impedance values for both HSPEs. Nevertheless, the HSPE containing 3% DVS consistently exhibits slightly lower impedance than the 5% DVS counterpart (Figure 5b–d vs. Figure 5f–h). As reported in Figure S1, the resistance values of pristine, 3% DVS, and 5% DVS HSPEs were compared. Pristine HSPE initially exhibits lower overall impedance, including both charge-transfer and SEI resistances; however, these values increase significantly after 12 h of operation. In contrast, the DVS-containing HSPEs show higher initial resistance, but maintain stable impedance over prolonged cycling up to 600 h. This stable, long-term behavior supports the proposed hypothesis that DVS enhances interfacial stability. The observed variations in overpotential and internal resistance can be attributed to the DVS reaction at the lithium metal interface, which may promote the formation of a thicker SEI, particularly at higher DVS contents [33–35]. This modification of the SEI is associated with the ability of sulfoxide compounds to polymerize in the presence of alkali metal, leading to the formation of a protective layer that prevents side-reaction and suppresses dendrite formation [36].

Ionic conductivity was measured for all HSPEs over a temperature range from −20°C to 70°C to evaluate the effect of DVS incorporation on ion mobility (Figure 6a). As expected, ionic conductivity decreases slightly with increasing DVS content, primarily due to the partial replacement of the ionic liquid and partial SEI formation. Despite this trend, all HSPE membranes exhibit high ionic conductivity over the entire temperature range, surpassing 1 mS cm^{-1} at 25°C and approaching ~5 mS cm^{-1} at 70°C. Consistent with the higher ionic liquid substitution and the formation of a partial resistive layer by DVS, the HSPE containing 5% DVS exhibits lower conductivity compared to both the 3% DVS and pristine samples.

The ESW of the HSPEs containing 3% and 5% DVS was first assessed by linear sweep voltammetry (LSV) to determine the anodic onset of electrolyte decomposition. As shown in Figure 6b, both DVS-containing HSPEs exhibit excellent oxidative stability, maintaining a low and stable current response up to approximately 4.8 V versus Li^+/Li. Based on a current density threshold of 5 μA cm^{-2}, these results confirm the suitability of the developed electrolytes for application with high-energy 4V-class cathode materials. To more precisely identify the breakdown voltage, chronoamperometric measurements were performed by applying a series of fixed potentials for 1 h each. As shown in Figure 6c, HSPEs containing 3% and 5% DVS exhibit a stable current response at 4.8 V versus Li^+/Li throughout the test. This behavior highlights the extended electrochemical stability window of the HSPEs.

Following the evaluation of the ESW, the galvanostatic charge–discharge behavior of DVS-containing HSPEs was investigated in SSLMB cells at ambient laboratory temperature employing a high-energy 4V-class NMC811 cathode (Figure 7). Rate capability tests were conducted within a voltage window of 3.0–4.2 V versus Li^+/Li by progressively varying the current rate from C/40 to C/2 and, subsequently, returning to C/20 (Figure 7a–c). During the initial cycle at C/40, the cell assembled with the 3% DVS HSPE delivers a near-complete practical capacity of approximately 180 mAh g^{-1}, with an initial Coulombic efficiency (iCE) of 87%. Upon increasing the current density, the cell retains high discharge capacities of 133, 115, 97, and 68 mAh g^{-1} at C/20, C/10, C/5, and C/2, respectively, while maintaining a CE close to 99%. These results further highlight the enhanced performance of the DVS-containing HSPE compared to the pristine HSPE in full-cell tests, as reported in Figure S2. In comparison, the HSPE containing 5% DVS exhibits slightly lower capacities across all tested rates, *viz.* about 167 mAh g^{-1} at C/40 (iCE of 83%), followed by 125, 113, 90, and 55 mAh g^{-1} at increasing C-rates up to C/2, with similarly high

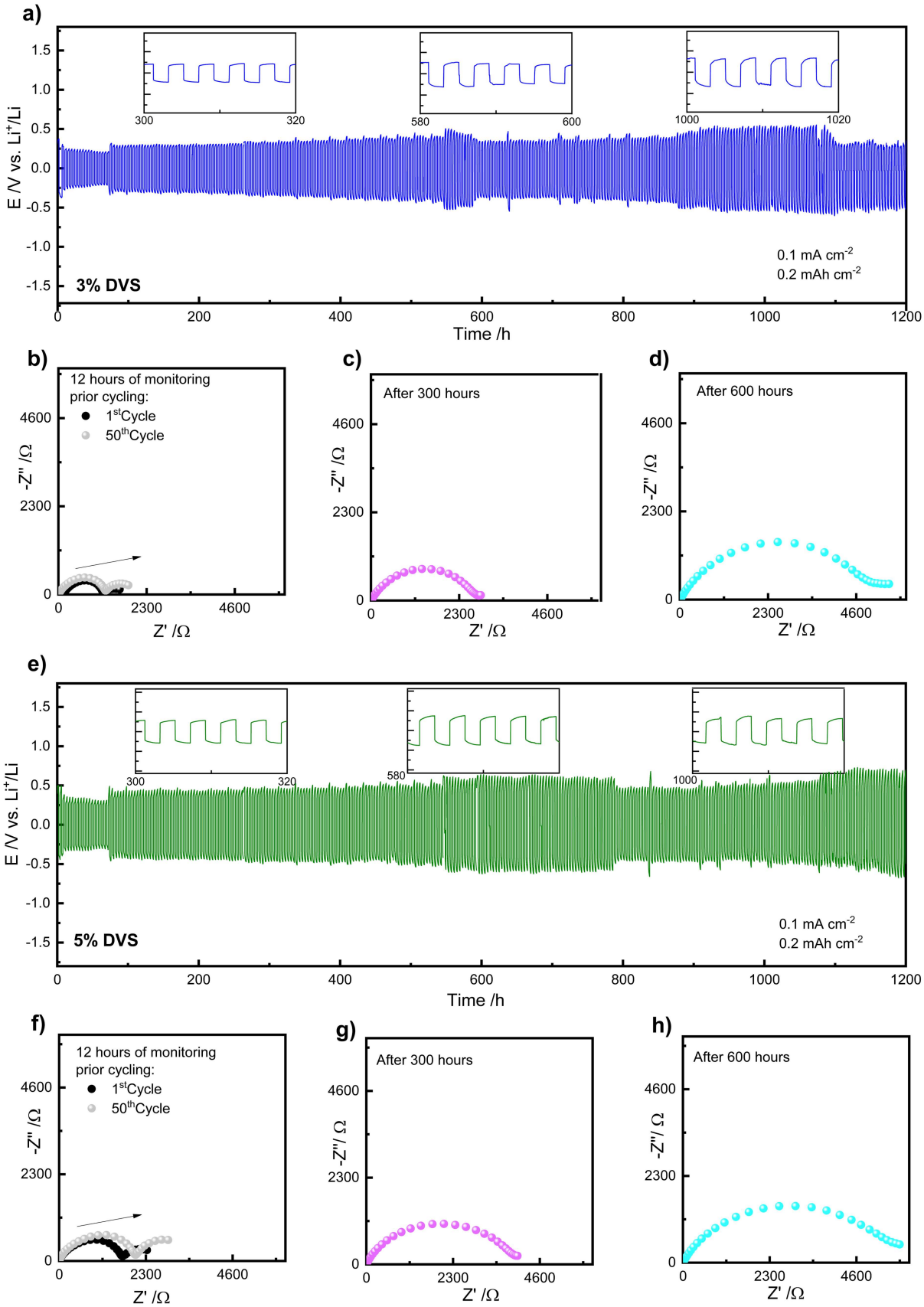

FIGURE 5 | Long-term galvanostatic lithium plating/stripping cycling and corresponding Nyquist plots measured at ambient laboratory temperature using HSPEs containing (a–d) 3% DVS and (e–h) 5% DVS. Tests were performed at a current density of 0.1 mA cm^{-2}, with plated/stripped areal capacity of 0.2 mAh cm^{-2} per half-cycle.

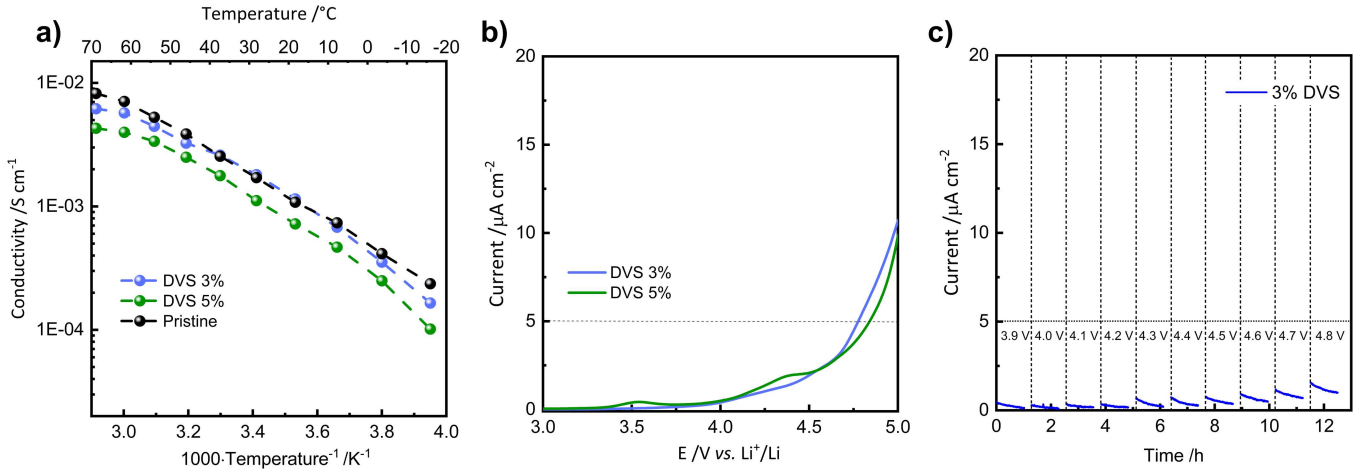

FIGURE 6 | (a) Arrhenius plots of ionic conductivity as a function of inverse temperature determined by EIS; (b) linear sweep voltammetry (LSV) measured at ambient laboratory temperature with a scan rate of 0.1 mV s^{-1}; and (c) chronoamperometry (CA) at stepwise potentials in the range of 3.3–4.8 V for the HSPEs under study.

CE (~99%) (Figure 7a and Figure S3). The reduced capacity observed for the HSPE 5% DVS is consistent with its slightly reduced ionic conductivity and corresponding higher overpotential measured in lithium plating/stripping experiments using symmetric cells. It is attributed to the formation of a thicker SEI, which becomes more pronounced at higher DVS contents and increases interfacial resistance. Overall, these results highlight the remarkable rate performance of the developed HSPE-based solid-state cells, which preserve substantial specific capacity even under elevated current densities. Moreover, as shown in Figure 7b,c, the voltage polarization remains limited over the entire range of applied C-rates, including practical C/2 current rate, indicating favorable kinetic behavior and stable reversible constant-current SSLMB cycling [37–39].

To further investigate the interfacial kinetics, EIS was performed on cells assembled with 3% or 5% DVS HSPEs, both after the activation stage (5th cycle) and following extended constant current cycling. As shown in Figure 7d,e, the Nyquist plots of both cells display comparable electrochemical features. Specifically: (i) the high-frequency intercept on the real axis corresponding to the bulk ionic resistance of the HSPE (R_s), which is governed by the electrolyte's ionic conductivity and thickness; (ii) the overlapping semicircles in the high- to mid-frequency region are attributed to interfacial resistances (R_{int1}+R_{int2}), associated with charge-transfer processes at the electrode–electrolyte interfaces; and (iii) the inclined line observed at low frequencies representing the Warburg diffusion element (W), which reflects Li^+ diffusion toward the blocking electrode [40–42]. As can be observed, the Nyquist plots of the HSPEs containing 3% or 5% DVS both exhibit a downward shift after prolonged cycling, indicating progressive interfacial stabilization and enhanced ionic liquid percolation within the working electrode porosity. The spectra were fitted using the equivalent circuit shown in Figure 7f. The fitting results reveal consistent trends for both systems: R_s remains unchanged, while R_{int1}+R_{int2} decreases after extended cycling, reflecting improved interphase stability and ionic transport at the electrode–electrolyte interface. Notably, the interfacial resistance measured after the fifth cycle is lower for the HSPE containing 3% DVS compared to that with 5% DVS, indicating more favorable interfacial kinetics at the lower additive concentration, well in line with the previously discussed results.

As shown in Figure 7g,h, both discharge curves exhibit a well-defined voltage step at approximately 3.67 V versus Li^+/Li during the first discharge at C/20 for both HSPE-based cells. This plateau position was determined from the corresponding d^2Q/dV^2 versus voltage plots [43, 44]. After 30 cycles, the discharge plateau shows negligible shifts to around 3.65 V for both cells, indicating no significant change in the Li^+ intercalation/deintercalation activity and suggesting stable electrochemical behavior in the 3.0–4.2 V versus Li^+/Li voltage window. In contrast, the cell operated up to 4.3 V vs Li^+/Li with the 3% DVS-based HSPE shows a noticeably sloped discharge profile, shifting from approximately 3.59 to 3.54 V. This behavior is chiefly ascribed to bulk structural degradation of the active material upon repeated cycling at the higher cut-off voltage [43, 44], also supported by the cycling behavior of the commercial NMC811 cathode in laboratory-scale cells with standard $LiPF_6$-based liquid electrolyte (Figure S4). As shown in Figure 6b,c, the ESW of the HSPE extends up to 4.8 V versus Li^+/Li, as confirmed by CA measurements under prolonged polarization, suggesting that electrolyte oxidation is not the dominant factor under the tested conditions. Consistently, the capacity fading observed after 30 cycles is more pronounced for the cell with an upper cut-off voltage of 4.3 V versus Li^+/Li compared to the cell cycled up to 4.2 V. Thus, the additive-enhanced HSPEs demonstrate excellent electrochemical performance in laboratory-scale SSLMB cells employing high-energy 4V-class NMC811 cathodes, confirming that the incorporation of DVS effectively stabilizes PVDF-HFP/IL-based electrolytes. This stabilization supports the development of high-voltage, intrinsically safe, and high-performance next-generation SSLMB conceived for practical operation in high-energy devices at ambient conditions.

4 | Conclusions

In this work, mechanically robust and self-supporting hybrid solid polymer electrolytes (HSPEs) were developed using a solvent-free fabrication strategy compatible with energy-efficient and scalable ASSLMB manufacturing. HSPEs are based

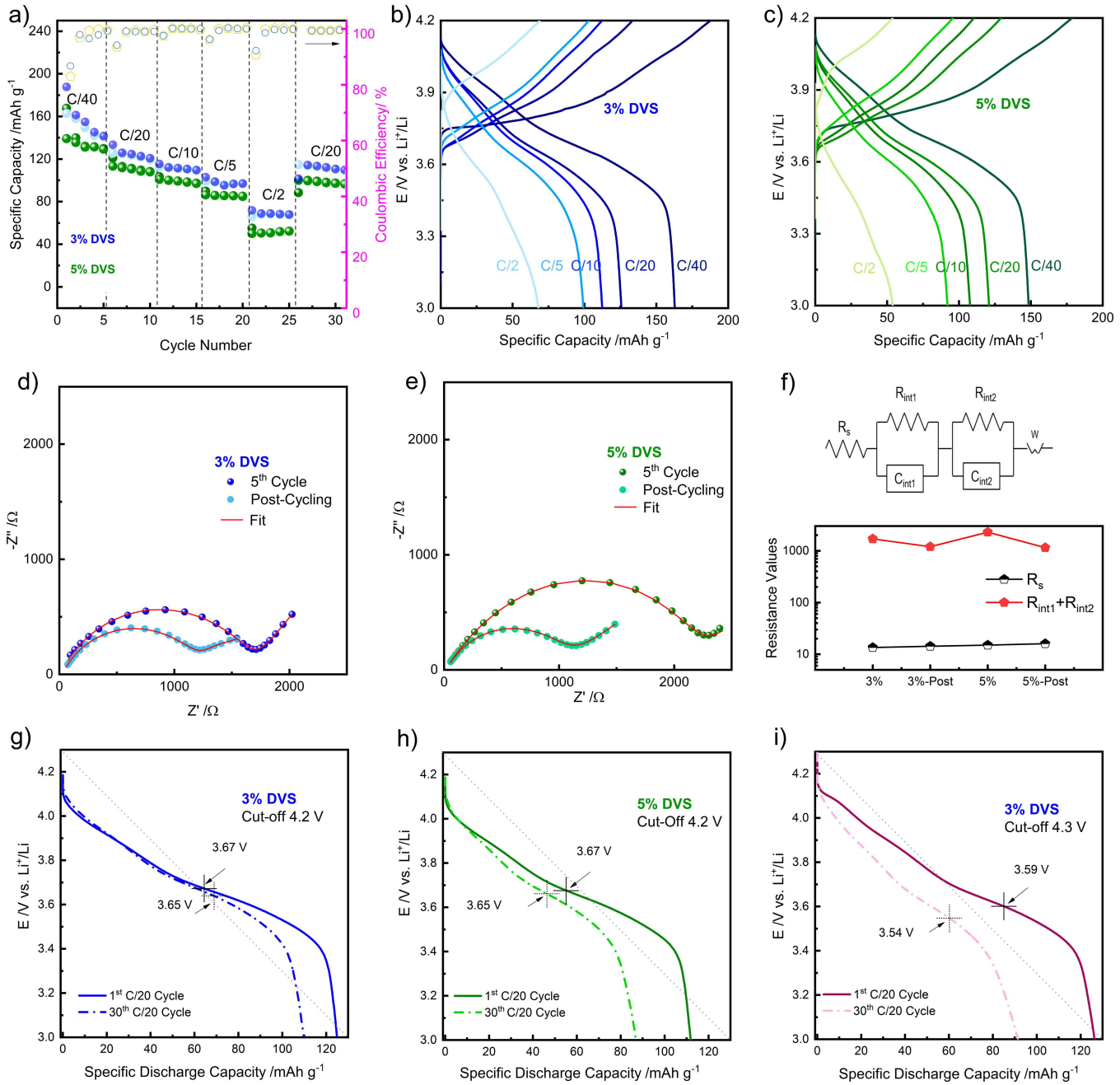

FIGURE 7 | Rate capability of Li||HSPE||NMC811 cells employing HSPEs containing 3% (blue) or 5% (green) DVS at ambient laboratory temperature (a), with corresponding voltage profiles versus specific capacity for the 3% DVS-based (b) and 5% DVS-based HSPEs (c) at different current rates (C/40, C/20, C/10, C/5, and C/2). Nyquist plots of the cells (d, e) and the equivalent circuit used for fitting, along with the corresponding resistance values (f). Discharge curves for the first cycle and after 30 cycles, with voltage plateaus calculated from d^2Q/dV^2 versus voltage, for 3% (blue) or 5% (green) DVS at 4.2 V (g,h) and for 3% DVS at 4.3 V (red) (i).

on a PVDF-HFP matrix plasticized with a pyrrolidinium-based IL ($Pyr_{14}FSI$) and added with little amounts of DVS as a functional interfacial stabilizer. They all exhibit a favorable combination of high ionic conductivity, mechanical robustness, and thermal stability. Indeed, while $Pyr_{14}FSI$ ensures efficient Li^+ ion mobility and contributes to thermal stability, the controlled introduction of DVS (3 or 5 wt%) plays a key role in stabilizing the SEI layer and suppressing interfacial degradation. Both DVS-containing HSPE membranes enable stable lithium plating and stripping in symmetric Li||Li cells, sustaining continuous operation for the whole test (up to 1200 h) at room temperature with a fixed plated/stripped capacity of 0.2 mAh cm^{-2} per half cycle. An increase in overpotential is observed at higher DVS content, indicating a trade-off between interfacial stabilization and charge-transfer resistance. In addition, laboratory-scale SSLM cells incorporating high-energy 4V-class NMC811 cathodes demonstrate excellent electrochemical performance under ambient conditions. Collectively, these results highlight the effectiveness of DVS in enhancing the interfacial stability of PVDF-HFP/$Pyr_{14}FSI$-based electrolytes, offering a promising pathway toward safe, high-voltage, and high-performance SSLMBs.

Acknowledgements

The SOLVE project (https://www.solveproject.eu/) has received funding from the European Union's Horizon EU Research and Innovation Program under grant agreement No 101147094. Support by MASE - ENEA program Ricerca di Sistema Elettrico (RDS) - Piano Triennale di Realizzazione (PTR) 2025-27 is gratefully acknowledged. Open access publishing facilitated by Politecnico di Torino, as part of the Wiley - CRUI-CARE agreement.

Conflicts of Interest

The authors declare no conflicts of interest.

Data Availability Statement

The data that support the findings of this study are available from the corresponding author upon reasonable request.

References

1. H. Darjazi, M. Falco, F. Colò, et al., "Electrolytes for Sodium Ion Batteries: The Current Transition From Liquid to Solid and Hybrid Systems," *Advanced Materials* 36 (2024): 2313572, https://doi.org/10.1002/adma.202313572.

2. G. Kumar, R. Singh, P. Chand, M. Kumar, R. R. Singh, and A. Kumar, "A Review on Polymer Electrolyte Materials in Context to Modifications in PVDF-HFP Polymer Host," *Journal of Solid State Electrochemistry* 29 (2025): 4493–4528, https://doi.org/10.1007/s10008-025-06343-9.

3. J. Wang, B. Ge, H. Li, et al., "Challenges and Progresses of Lithium-Metal Batteries," *Chemical Engineering Journal* 420 (2021): 129739, https://doi.org/10.1016/j.cej.2021.129739.

4. Z. Liu, X. Fu, Z. Li, et al., "Integrated Anode With 3D Electron/Ion Conductive Network for Stable Lithium Metal Batteries," *Energy Storage Materials* 66 (2024): 103201, https://doi.org/10.1016/j.ensm.2024.103201.

5. X. B. Cheng, R. Zhang, C. Z. Zhao, and Q. Zhang, "Toward Safe Lithium Metal Anode in Rechargeable Batteries: A Review," *Chemical Reviews* 117 (2017): 10403–10473, https://doi.org/10.1021/acs.chemrev.7b00115.

6. S. Kim, G. Park, S. J. Lee, et al., "Lithium-Metal Batteries: From Fundamental Research to Industrialization," *Advanced Materials* 35 (2023): 1–20, https://doi.org/10.1002/adma.202206625.

7. J. Mindemark, B. Sun, E. Törmä, and D. Brandell, "High-Performance Solid Polymer Electrolytes for Lithium Batteries Operational at Ambient Temperature," *Journal of Power Sources* 298 (2015): 166–170, https://doi.org/10.1016/j.jpowsour.2015.08.035.

8. L. Balducci, H. Darjazi, A. Piovano, G. A. Elia, and C. Gerbaldi, "On the Role of UV Crosslinking to Enhance Moderate-Temperature Operation of Truly Solid-State Li-Metal Batteries Based on Recycled-PVB-Modified Polyether Electrolytes," *Journal of Power Sources* 662 (2026): 238704, https://doi.org/10.1016/j.jpowsour.2025.238704.

9. A. Patriarchi, H. Darjazi, A. Piovano, et al., "Unlocking Sustainable-By-Design Li-Metal Batteries by Recycled PVB in Blend Polymer Electrolytes," *Chemsuschem* 18 (2025): e202501288, https://doi.org/10.1002/cssc.202501288.

10. F. Gambino, M. Gastaldi, A. Jouhara, et al., "Formulating PEO-Polycarbonate Blends as Solid Polymer Electrolytes by Solvent-Free Extrusion," *Journal of Power Sources Advances* 30 (2024): 100160, https://doi.org/10.1016/j.powera.2024.100160.

11. M. Z. Kufian, M. F. Aziz, M. F. Shukur, et al., "PMMA – LiBOB Gel Electrolyte for Application in Lithium Ion Batteries," *Solid State Ionics* 208 (2012): 36–42, https://doi.org/10.1016/j.ssi.2011.11.032.

12. Y. Liu, T. Yang, R. Fang, et al., "Ultra-Homogeneous Dense Ag Nano Layer Enables Long Lifespan Solid-State Lithium Metal Batteries," *Journal of Energy Chemistry* 96 (2024): 110–119, https://doi.org/10.1016/j.jechem.2024.04.017.

13. R. Bajaj, H. Darjazi, M. Gastaldi, L. Balducci, G. A. Elia, and C. Gerbaldi, "Role of Cyclic Carbonates in Enhancing UV-Crosslinked PEO-PEC Electrolytes for Room-Temperature Lithium Metal Batteries," *Journal of Power Sources* 674 (2026): 239777, https://doi.org/10.1016/j.jpowsour.2026.239777.

14. Y. Liu, D. Yang, R. Xu, et al., "Synergistic Regulation of Bulk and Interfacial Properties in PEO Electrolyte Using CaF_2 for Stable Lithium Metal Batteries," *Journal of Materials Chemistry A* 14 (2026): 13552–13563, https://doi.org/10.1039/D5TA09885H.

15. M. Jabeen, M. Ishaq, S. Zhao, et al., "Thermally Adaptive PVDF-HFP/Ionic Liquid Electrolyte Enabling Stable SEI/CEI Formation in Sodium Metal Batteries," *Advance Functional Materials* 25343 (2026): 1–12, https://doi.org/10.1002/adfm.202525343.

16. S. Caimi, H. Wu, and M. Morbidelli, "PVDF-HFP and Ionic-Liquid-Based, Freestanding Thin Separator for Lithium-Ion Batteries," *ACS Applied Energy Materials* 1 (2018): 5224–5232, https://doi.org/10.1021/acsaem.8b00860.

17. I. Hasa, S. Passerini, and J. Hassoun, "Characteristics of an Ionic Liquid Electrolyte for Sodium-Ion Batteries," *Journal of Power Sources* 303 (2016): 203–207, https://doi.org/10.1016/j.jpowsour.2015.10.100.

18. M. Armand, F. Endres, D. R. MacFarlane, H. Ohno, and B. Scrosati, "Ionic-Liquid Materials for the Electrochemical Challenges of the Future," *Nature Materials* 8 (2009): 621–629, https://doi.org/10.1038/nmat2448.

19. Q. Zhou, W. A. Henderson, G. B. Appetecchi, M. Montanino, and S. Passerini, "Physical and Electrochemical Properties of N-Alkyl-N-Methylpyrrolidinium Bis(Fluorosulfonyl)Imide Ionic Liquids: PY13FSI and PY 14FSI," *Journal of Physical Chemistry B* 112 (2008): 13577–13580, https://doi.org/10.1021/jp805419f.

20. H. Zhang, G. G. Eshetu, X. Judez, C. Li, L. M. Rodriguez-Martínez, and M. Armand, "Electrolyte Additives for Lithium Metal Anodes and Rechargeable Lithium Metal Batteries: Progress and Perspectives," *Angewandte Chemie International Edition* 57 (2018): 15002–15027, https://doi.org/10.1002/anie.201712702.

21. B. Tong, Z. Song, H. Wan, et al., "Sulfur-Containing Compounds as Electrolyte Additives for Lithium-Ion Batteries," *InfoMat* 3 (2021): 1364–1392, https://doi.org/10.1002/inf2.12235.

22. P. Jankowski, N. Lindahl, J. Weidow, W. Wieczorek, and P. Johansson, "Impact of Sulfur-Containing Additives on Lithium-Ion Battery Performance: From Computational Predictions to Full-Cell Assessments," *ACS Applied Energy Materials* 1 (2018): 2582–2591, https://doi.org/10.1021/acsaem.8b00295.

23. D. Yang, Y. Liu, T. Yang, et al., "Anti-Corrosion Lithium Anode Interface by $Li_{6.4}La_3Zr_{1.4}Ta_{0.6}O_{12}$ Modified Buffer Layer for Stable Cycling of Room-Temperature Solid-State Lithium Metal Batteries," *Journal of Colloid and Interface Science* 689 (2025): 137225, https://doi.org/10.1016/j.jcis.2025.03.014.

24. Y. Liu, D. Yang, R. Xu, et al., "Synergistic Regulation of Bulk and Interfacial Properties in PEO Electrolyte Using CaF2for Stable Lithium Metal Batteries," *Journal of Materials Chemistry A* 14 (2026): 13552–13563, https://doi.org/10.1039/d5ta09885h.

25. K. Polat, "Energy Harvesting From a Thin Polymeric Film Based on PVDF-HFP and PMMA Blend," *Applied Physics A* 126 (2020): 497, https://doi.org/10.1007/s00339-020-03698-w.

26. J. Sharma, C. Totee, V. Kulshrestha, and B. Ameduri, "Spectroscopic Evidence and Mechanistic Insights on Dehydrofluorination of PVDF in Alkaline Medium," *European Polymer Journal* 201 (2023): 112580, https://doi.org/10.1016/j.eurpolymj.2023.112580.

27. X. Cai, T. Lei, D. Sun, and L. Lin, "A Critical Analysis of the α, β and γ Phases in Poly(Vinylidene Fluoride) Using FTIR," *RSC Advances* 7 (2017): 15382–15389, https://doi.org/10.1039/C7RA01267E.

28. J. Huang and A. F. Hollenkamp, "Thermal Behavior of Ionic Liquids Containing the FSI Anion and the Li+Cation," *Journal of Physical*

Chemistry C 114 (2010): 21840–21847, https://doi.org/10.1021/jp107740p.

29. G. B. Appetecchi, S. Scaccia, C. Tizzani, F. Alessandrini, and S. Passerini, "Synthesis of Hydrophobic Ionic Liquids for Electrochemical Applications," *Journal of the Electrochemical Society* 153 (2006): A1685, https://doi.org/10.1149/1.2213420.

30. I. Hargittai, B. Rozsondai, B. Nagel, P. Bulcke, G. Robinet and J.-F. Labarre, "Molecular Structure of Divinyl Sulphone as Studied by Electron Dif- Fraction,Vibrational Spectroscopy, and Semiempirical CN D0/2 Molecular- Orbital Calculations," *Journal of Chemical Society Dalton* 7 (1978): 861–868, https://doi.org/10.1039/DT9780000861.

31. B. Tong, Z. Song, H. Wan, et al., "Sulfur-Containing Compounds as Electrolyte Additives for Lithium-Ion Batteries," *InfoMat* 3 (2021): 1364–1392, Object Identifier (DOI) https://doi.org/10.1002/inf2.12235Digital.

32. C. H. Du, B. K. Zhu, and Y. Y. Xu, "The Effects of Quenching on the Phase Structure of Vinylidene Fluoride Segments in PVDF-HFP Copolymer and PVDF-HFP/PMMA Blends," *Journal of Materials Science* 41 (2006): 417–421, https://doi.org/10.1007/s10853-005-2182-6.

33. G. Kang, G. Zhong, K. Cai, et al., "Dimethyl Sulfide Electrolyte Additive Enabled High-Voltage Lithium-Ion Battery," *ACS Energy Letters* 9 (2024): 2572–2581, https://doi.org/10.1021/acsenergylett.4c00519.

34. Z. Xiu-Qing, S. Tang, and Y.-Z. Fu, "Recent Advances of Functional Electrolyte Additives for Lithium-Sulfur Batteries," *Journal of Electrochemistry* 29 (2023): 1–12, https://doi.org/10.13208/j.electrochem.2217005.

35. S. Wang, H. Guo, X. Li, et al., "How Sulfur-Containing Additives Stabilize Electrode/Electrolyte Interface of High Voltage Graphite/Li-CoO2 Battery," *Applied Surface Science* 684 (2025): 161805, https://doi.org/10.1016/j.apsusc.2024.161805.

36. N. Ziegenbalg, L. Elbinger, U. S. Schubert, and J. C. Brendel, "Polymers From S-Vinyl Monomers: Reactivities and Properties," *Polymer Chemistry* 13 (2022): 5019–5041, https://doi.org/10.1039/D2PY00850E.

37. J. Xiong, T. Zheng, Y. J. Cheng, J. Sun, R. Cao, and Y. Xia, "Sulfur Is a New High-Performance Additive Toward High-Voltage $LiNi_{0.5}Co_{0.2}Mn_{0.3}O_2$ Cathode: Tiny Amount, Huge Impact," *ACS Applied Materials & Interfaces* 13 (2021): 18648–18657, https://doi.org/10.1021/acsami.1c00391.

38. M. A. Dato, J. Edgington, C. Hung, et al., "Sulfur Solutions: Advancing High Voltage and High Energy Lithium Batteries With Organosulfur Electrolytes," *Advance Energy Materials* 14 (2024): 1–38, https://doi.org/10.1002/aenm.202303794.

39. Z. Fan, X. Zhou, J. Qiu, et al., "Sulfur-Rich Additive-Induced Interphases Enable Highly Stable 4.6 V $LiNi_{0.5}Co_{0.2}Mn_{0.3}O_2$ ||Graphite Pouch Cells," *Angewandte Chemie International Edition* 62 (2023): e202308888, https://doi.org/10.1002/anie.202308888.

40. L. Balducci, H. Darjazi, E. Gonzalo, R. Cid, F. Bonilla, and F. Nobili, "Evaluation of Electronic–Ionic Transport Properties of a Mg/Zr-Modified $LiNi_{0.5}$ $Mn_{1.5}$ O_4 Cathode for Li-Ion Batteries," *ACS Applied Materials & Interfaces* 15 (2023): 55620–55632, https://doi.org/10.1021/acsami.3c10480.

41. M. Gastaldi, F. Gambino, H. Darjazi, et al., "Dry Extrusion of Poly (Ethylene Oxide)-Polycarbonate All-Solid-State Electrolytes for Li-Metal Batteries: Effect of UV-Crosslinking on the Electrochemical Performance," *Materials Today Energy* 52 (2025): 101947, https://doi.org/10.1016/j.mtener.2025.101947.

42. F. Gambino, M. Gastaldi, A. Jouhara, et al., "Formulating PEO-Polycarbonate Blends as Solid Polymer Electrolytes by Solvent-Free Extrusion," *Journal of Power Sources Advances* 30 (2024): 100160, https://doi.org/10.1016/j.powera.2024.100160.

43. H. Darjazi, S. J. Rezvani, S. Brutti, and F. Nobili, "Improvement of Structural and Electrochemical Properties of NMC Layered Cathode Material by Combined Doping and Coating," *Electrochimica Acta* 404 (2022): 139577, https://doi.org/10.1016/j.electacta.2021.139577.

44. Y. Ruan, X. Song, Y. Fu, C. Song, and V. Battaglia, "Structural Evolution and Capacity Degradation Mechanism of $LiNi_{0.6}Mn_{0.2}Co_{0.2}O_2$ Cathode Materials," *Journal of Power Sources* 400 (2018): 539–548, https://doi.org/10.1016/j.jpowsour.2018.08.056.

Supporting Information

Additional supporting information can be found online in the Supporting Information section.

Figure S1: Resistance values of pristine, 3% DVS, and 5% DVS HSPEs, derived from Nyquist plots.

Figure S2: Voltage vs. specific capacity profiles of Li‖HSPE‖NMC811 cells employing pristine HSPE at different current densities (C/40, C/20, C/10, C/5, and C/2) and ambient temperature.

Figure S3: Rate capability of Li‖HSPE‖NMC811 cells employing HSPEs containing 3% (blue) or 5% (green) DVS at room temperature at different current densities (C/40, C/20, C/10, C/5, and C/2).

Figure S4: Voltage vs. specific capacity profiles of NMC811 cells employing a $LiPF_6$-based liquid electrolyte at different current densities (C/20, C/10, C/5, C, and 2C) and ambient temperature.